JACS
JOURNAL OF THE AMERICAN CHEMICAL SOCIETY
pubs.acs.org/JACS
Article

Tiny Sc Allows the Chains to Rattle: Impact of Lu and Y Doping on the Charge-Density Wave in ScV_6Sn_6

William R. Meier,* Richa Pokharel Madhogaria, Shirin Mozaffari, Madalynn Marshall, David E. Graf, Michael A. McGuire, Hasitha W. Suriya Arachchige, Caleb L. Allen, Jeremy Driver, Huibo Cao, and David Mandrus*

Cite This: *J. Am. Chem. Soc.* 2023, 145, 20943−20950
Read Online
ACCESS | Metrics & More | Article Recommendations | Supporting Information

ABSTRACT: The kagome metals display an intriguing variety of electronic and magnetic phases arising from the connectivity of atoms on a kagome lattice. A growing number of these materials with vanadium−kagome nets host charge−density waves (CDWs) at low temperatures, including ScV_6Sn_6, CsV_3Sb_5, and V_3Sb_2. Curiously, only the Sc version of the RV_6Sn_6 materials with a $HfFe_6Ge_6$-type structure hosts a CDW (R = Gd−Lu, Y, Sc). In this study, we investigate the role of rare earth size in CDW formation in the RV_6Sn_6 compounds. Magnetization measurements on our single crystals of $(Sc,Lu)V_6Sn_6$ and $(Sc,Y)V_6Sn_6$ establish that the CDW is suppressed by substituting Sc by larger Lu or Y. Single-crystal X-ray diffraction reveals that compressible Sn−Sn bonds accommodate the larger rare earth atoms within loosely packed R−Sn−Sn chains without significantly expanding the lattice. We propose that Sc provides extra room in these chains crucial to CDW formation in ScV_6Sn_6. Our rattling chain model explains why both physical pressure and substitution by larger rare earth atoms hinder CDW formation despite opposite impacts on lattice size. We emphasize the cooperative effect of pressure and rare earth size by demonstrating that pressure further suppresses the CDW in a Lu-doped ScV_6Sn_6 crystal. Our model not only addresses why a CDW only forms in the RV_6Sn_6 materials with tiny Sc but also advances our understanding of why unusual CDWs form in the kagome metals.

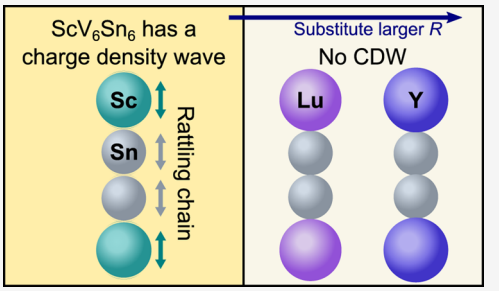

INTRODUCTION

A charge−density wave (CDW) is an ordered phase of a metallic crystal that appears on cooling. It is characterized by both the localization of some conduction electrons and an associated atomic displacement, which reduces the translational symmetry of the lattice.[1,2] CDWs show excellent tuneability with physical pressure, chemical composition, and disorder.[3−11] In fact, tuning the CDW transition to zero temperature is a good approach to discover new superconductors.[12−19]

Kagome metals have recently attracted significant interest for their unusual electronic and magnetic properties arising from kagome sheets of transition metals.[21−37] A growing number of these materials display a CDW at low temperatures, especially when vanadium forms the kagome net. The AV_3Sb_5 materials (A = K, Rb, Cs) host both superconductivity and curious CDW phases.[23−26,38−50] V_3Sb_2 likely has a CDW transition as well.[51]

A CDW has also been identified in the vanadium−kagome metal ScV_6Sn_6 below 92 K.[52] This is the Sc member of the rare earth RV_6Sn_6 compounds (R = Sc, Y, and Gd−Lu).[53−55] These adopt the hexagonal $HfFe_6Ge_6$ structure type (Figure 1a) characterized by V-kagome sheets interleaved between Sn2-honeycomb and Sn3-honeycomb sheets. Rare earth atoms and

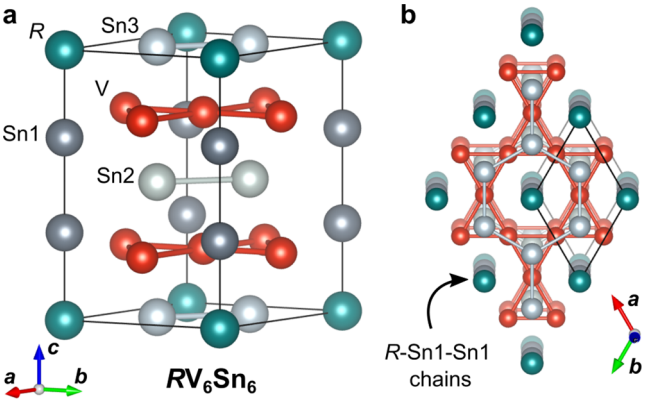

Figure 1. Crystal structure of the RV_6Sn_6 compounds. (a) Stacked vanadium−kagome and Sn2/Sn3-honeycomb sheets along the *c*-axis. (b) R−Sn1−Sn1 chains along *c* fill channels in honeycomb and kagome nets. Figures generated with VESTA.[20]

Received: June 16, 2023
Published: September 14, 2023

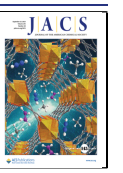

https://doi.org/10.1021/jacs.3c06394
J. Am. Chem. Soc. 2023, 145, 20943−20950

Sn1 atoms form a chain that occupies channels in the hexagonal holes in the kagome and honeycomb layers, as illustrated in Figure 1b. These chains of atoms play a pivotal role in the CDW mode as they displace along the *c*-axis in the modulated structure.[52,56] Several CDW modes appear to compete in ScV_6Sn_6[57] demonstrated by the strong CDW fluctuations observed above the transition temperature[56,58,59] with impacts on the electrical transport properties.[27]

It is important to note that the CDW in ScV_6Sn_6 has a $\left(\frac{1}{3}\frac{1}{3}\frac{1}{3}\right)$ wave vector[52,58,59] in contrast to that observed in the AV_3Sb_5 materials $\left(\frac{1}{2}\frac{1}{2}\frac{1}{2}\text{or}\frac{1}{2}\frac{1}{2}\frac{1}{4}\right)$.[23,25,40−43,60,61] Another key difference is that the CDW in AV_3Sb_5 compounds is dominated by vanadium displacements perpendicular to the hexagonal *c*-axis.[25] Numerous investigations of the electronic structure of ScV_6Sn_6 by photoemission measurements tie the CDW order to the Sn bands instead of the prominent vanadium bands.[59,62−66] There is evidence that the CDW phase has unusual characteristics including anomalous Hall-like responses[27,67] and claims of time reversal symmetry breaking.[68]

So far, none of the other RV_6Sn_6 appear to host CDW order.[27,54,55,69−72] What makes the scandium version special? One clue is that the CDW in ScV_6Sn_6 is suppressed by pressure and disappears before 2.4 GPa.[73] Maybe the lattice volume and rare earth size are important.

In this paper, we investigate the impact of rare earth size on CDW formation in RV_6Sn_6 materials by isovalent substitution of Lu and Y into ScV_6Sn_6. We synthesized single crystals of $(Sc_{1-x}Lu_x)V_6Sn_6$ and $(Sc_{1-y}Y_y)V_6Sn_6$ and determined the CDW transition temperature with magnetization measurements. We find that the CDW phase is suppressed in both cases without significant impact on the lattice size. Detailed crystallography reveals that larger *R* atoms are accommodated by extra room between the Sn1 and Sn1 atoms along the *c*-axis (Figure 1a).

We propose that this space in the loose R−Sn1−Sn1 chains is crucial for the CDW formation in ScV_6Sn_6. Our rattling chain model explains why the CDW is suppressed by pressure as well as by doping with larger rare earth atoms despite their opposite impacts on lattice volume. We test our model by confirming that pressure reduces the CDW transition temperature in a sample where the instability is already suppressed by Lu doping. This study answers why only the Sc version of the RV_6Sn_6 kagome metals hosts CDW order; the small Sc atoms provide extra room for R−Sn1−Sn1 chains to rattle and permit the CDW displacements. In addition, this system exhibits a deviation from the usual correspondence between chemical and physical pressure.

EXPERIMENTAL SECTION

Crystal Growth. Crystals of (Sc,Lu)V_6Sn_6 and (Sc,Y)V_6Sn_6 were grown from a Sn-rich melt following Arachchige et al.[52] Distilled scandium pieces (Alfa Aesar 99.9%), distilled Lutetium pieces (Alfa Aesar 99.9%), yttrium pieces (Alfa Aesar 99.9%), 3 mm pieces of vanadium slugs (Alfa Aesar 99.8%), and tin shot (Alfa Aesar 99.99+ %) were added to 2 or 5 mL alumina Canfield crucible sets.[74] An atomic ratio of Sc/Lu/V/Sn or Sc/Y/V/Sn = $(1 - r)/r/6/60$ was used for all growths. The crucibles were sealed in silica ampules filled with about 0.2 atm argon. These were heated in a box furnace to 1150 °C over 12 h and held for 15 h to dissolve as much vanadium as possible. Crystals were grown during a 300 h slow cool to 780 °C. The ampules were then removed from the furnace, inverted into a centrifuge, and spun rapidly to fling the remaining liquid away from the crystals.

These growths yielded hard, light-gray metallic hexagonal crystals on crucible walls and vanadium pieces. Mirror-like basal, prismatic, and pyramidal facets are common. The Sc- and Lu-rich crystals were 0.3 and 3 mm in size and tend to be blocky with some Sn inclusions. The most Y-rich crystals formed flatter hexagonal plates.

Characterization. Powder X-ray diffraction (XRD) was carried out using a Bruker D2 Phaser with a Cu Kα source and Ni filter for phase identification and to determine lattice parameters.

Single-crystal X-ray diffraction measurements at room temperature were carried out using a Rigaku XtaLAB PRO diffractometer. Data collection and integration were done using the Rigaku Oxford Diffraction CrysAlis Pro software[75] and the structural refinement was performed using a SHELXTL package.[76,77] Refined structures and .cif files of LuV_6Sn_6 and YV_6Sn_6 can be found in the Supporting Information.

Energy-dispersive spectroscopy (EDS) was performed to estimate the ratios of the rare earth elements. Crystals were mounted in Crystalbond and polished flat. EDS was carried out with a Zeiss EVO scanning electron microscope at 20 keV.

Magnetization measurements were carried out using a Quantum Design Magnetic Property Measurement System 3 with the Vibrating Sample Magnetometer (VSM) option. Crystals were etched in an aqueous 10 wt % HCl solution for 12−36 h to remove surface Sn and then attached to a fused silica paddle with GE varnish. All measurements presented were measured with the field perpendicular to the hexagonal *c*-axis. The fraction of superconducting Sn in each sample was estimated by a 10 Oe zero-field-cooled measurement through the transition. Estimated β-Sn fractions ranged from 0.5−7 vol %.

To check for superconductivity, resistance measurements down to 0.12 K were performed using the Adiabatic Demagnetization Refrigerator (ADR) option in the Quantum Design Physical Property Measurement System using silver paste and platinum wire contacts. ADR resistivity measurements revealed no evidence of superconductivity down to at least 150 mK in Lu-doped ScV_6Sn_6 samples. These results are presented in the Supporting Information.

Two single crystals of $(Sc_{1-x}Lu_x)V_6Sn_6$ and one LuV_6Sn_6 crystal were measured concurrently in the same piston-cylinder pressure cell. Contacts were made between the platinum wire and the samples using Epotek H20E silver epoxy, which was cured at 135 °C for 30 min. Daphne 7575 was used as a pressure medium,[78] and the value of the pressure was calibrated using the fluorescence of a small ruby chip located near the crystals.[79] The pressure was recorded at room temperature and again at low temperature by comparing it with the values of fluorescence peaks from a ruby sample at ambient pressure. Resistance measurements were made for each sample using a Lakeshore 372 resistance bridge with a 3708 preamp/scanner. The pressure cell was loaded into a Quantum Design Physical Property Measurement System (PPMS) for temperature control with about 50 Torr of helium exchange gas in the sample chamber. All measurements were done with a cooling and warming rate of 0.5 K min^{-1}. A calibrated Cernox thermometer was fixed on the outside of the pressure cell next to the copper sample wires to accurately determine the temperature of the measured crystals.

RESULTS AND DISCUSSION

Lattice Trends. Figure 2 presents the evolution of the lattice parameters as Y and Lu are doped into ScV_6Sn_6. *a* and *c* vary continuously across both series, indicating that a complete solid solutions exists. *a* increases linearly across with 0.52 and 0.88% expansion to LuV_6Sn_6 and YV_6Sn_6, respectively. The *c* parameter increases weakly with Y doping (0.10%) and subtly decreases for the Lu series (−0.02%). Ionic radii provide an imperfect proxy of the size of the R atoms in RV_6Sn_6. The radii of Sc^{3+}, Lu^{3+}, and Y^{3+} are quoted as 0.87, 0.977, and 1.019 Å at 8-coordinated sites in oxide materials.[80] Considering that the

https://doi.org/10.1021/jacs.3c06394
J. Am. Chem. Soc. 2023, 145, 20943−20950

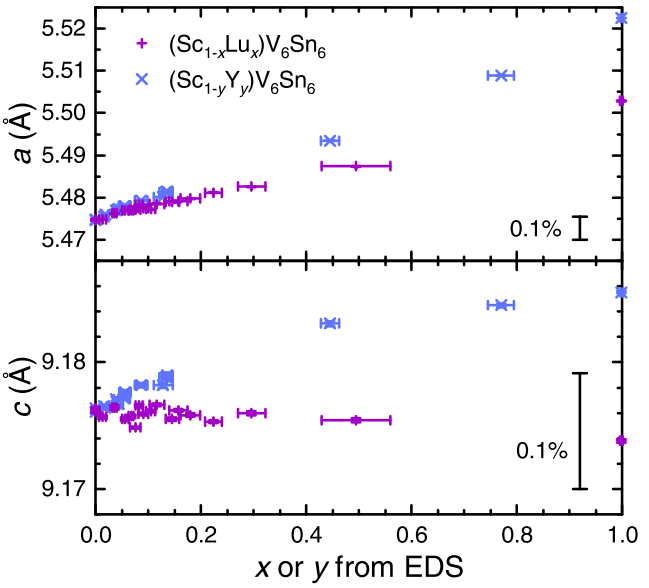

Figure 2. Variation of lattice parameters for the $(Sc_{1-x}Lu_x)V_6Sn_6$ and $(Sc_{1-y}Y_y)V_6Sn_6$ doping series. Horizontal error bars represent the standard deviations of measured x and y by EDS. Vertical error bars are the standard uncertainties from refinements of the lattice parameters. Black vertical bars communicate the size of a 0.1% change in lattice parameters.

Lu and Y ions are 12 and 17% larger than Sc, it is surprising that the changes in the c lattice parameter are so weak across the substitution series. This suggests that some other aspect of the structure is setting the lattice size.

Magnetization. Next, we will explore how Lu and Y substitution impacts the CDW in ScV_6Sn_6. Figure 3 presents the normalized magnetization curves for selected Lu- and Y-doped samples. The magnitude of the susceptibility at room temperature is comparable for all samples measured, ranging from 7.5−9.0 × 10^{-7} emu g^{-1} Oe^{1-} (6.2−8.2 × 10^{-5} cm^3(mol atom)$^{-1}$) consistent with Pauli paramagnetism.[81] The CDW transition in ScV_6Sn_6 manifests as a sharp drop of susceptibility on cooling through the first-order transition.[52] This signature begins at 94 K (black) and shifts to lower temperatures with increasing Lu or Y content. At the same time, the size of the drop decreases. The broadening of the transition step is likely due to the chemical inhomogeneity observed by EDS.

Phase Diagrams. Figure 4a,b summarizes suppression of the CDW phase with Lu and Y substitution extracted from magnetization. T_{CDW} falls smoothly and then discontinuously around a critical doping ($x \approx 0.13$ and $y \approx 0.07$), where we lose the step-like signature. This is not the usual behavior we expect for a quantum critical point where the transition temperature is smoothly reduced to 0 K.[82] Instead, our CDW transition is first order, so the phase can disappear more abruptly. It is possible that the transition has broadened so it is no longer visible as in $MgCo_6Ge_6$,[83] but the reduction in symmetry by a CDW requires a transition. No new transitions are observed with higher values of x and y.

It is important to note that less Y is required to destroy the CDW than Lu. This might arise from yttrium's larger size. Figure 4c shows that the trend of T_{CDW} versus the average R^{3+} ionic radius has similar behavior for the Lu and Y series. The Lu and Y are also heavier atoms than Sc (174.97, 88.906, and 44.956 g mol^{-1}, respectively). Rare earth mass could be playing a role in suppressing the CDW as proposed by Hu et al.[66] We

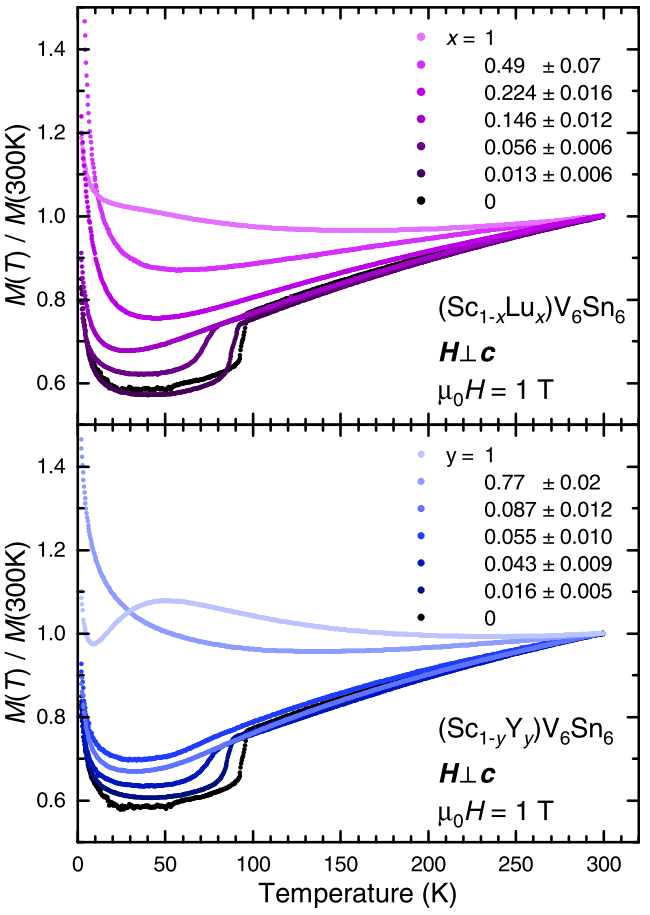

Figure 3. Normalized magnetization vs temperature curves for selected Lu- and Y-doped ScV_6Sn_6 crystals. All curves presented were measured on warming after cooling in zero magnetic field.

suggest that this is less important than size because Lu is heavier than Y, yet we observe that less Y is needed to destabilize the CDW.

Suppression of a CDW can lead to superconductivity. ADR resistivity measurements revealed no evidence of superconductivity down to at least 150 mK in Lu-doped samples with $x = 0.157 \pm 0.017$ and 0.180 ± 0.019, as well as Y-doped samples with $y = 0.055 \pm 0.010$ and 0.087 ± 0.012 (see the Supporting Information).

Chemical vs Physical Pressure. To simplify our understanding of the evolution of phase transitions, we often consider that chemical and mechanical pressure have the same impact on the electronic and lattice subsystems. If the lattice volume has a strong impact on the stability of a phase, then we might expect the transition temperature to rise as we expand the lattice with doping (negative chemical pressure) and fall as we compress the lattice mechanically or through doping.

This correspondence between chemical and physical pressure is epitomized by the CDW and superconducting 3−4−13 Remeika phases. Specifically, the $(Sr,Ca)_3Ir_4Sn_{13}$ and $(Sr,Ca)_3Rh_4Sn_{13}$ substitution series (chemical pressure) exhibit common evolution of the CDW and superconducting critical temperatures with physical pressure.[10,11]

Our investigation of the CDW evolution in isovalently doped ScV_6Sn_6 reveals behavior that deviates from the chemical−physical pressure picture. We observe that the T_{CDW} decreases with negative chemical pressure as we

https://doi.org/10.1021/jacs.3c06394
J. Am. Chem. Soc. 2023, 145, 20943−20950

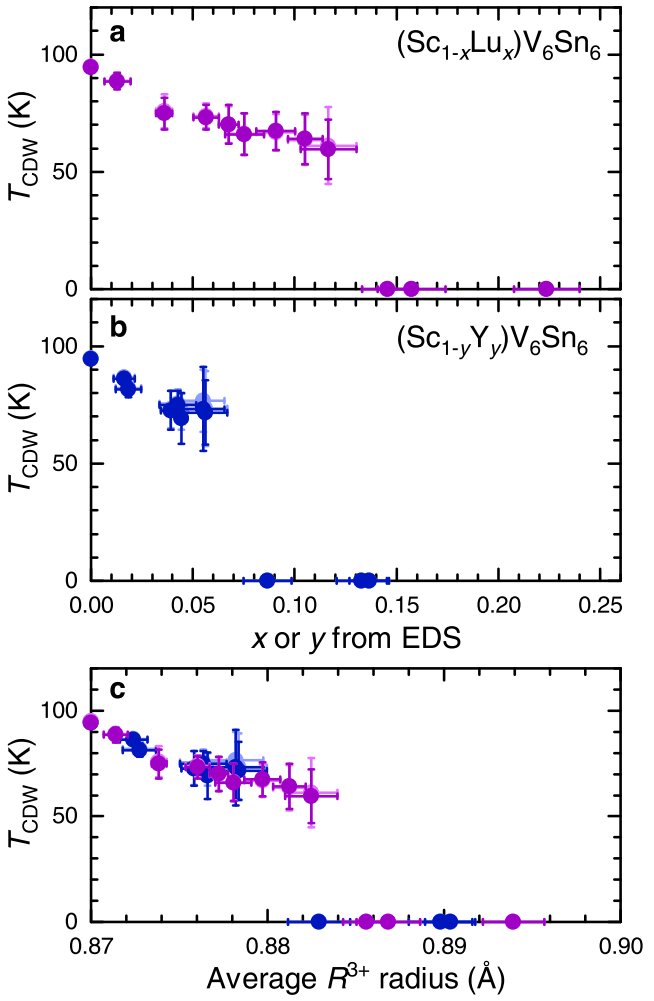

Figure 4. Evolution of T_{CDW} with Lu and Y doping of ScV_6Sn_6. (a, b) Charge density wave temperature (T_{CDW}) vs composition. Horizontal error bars represent standard deviations of Lu/(Sc + Lu) and Y/(Sc + Y) determined by EDS. Vertical bars represent the estimated transition width of the transition based on the drop in the $M(T)$ measurements (Supporting Information). Light and dark symbols represent the transition observed on warming and cooling, respectively. (c) T_{CDW} vs average ionic radius of the R atoms.[80]

substitute in the larger Lu and Y atoms (Figure 4). Zhang et al. reveal that physical pressure also reduces T_{CDW}.[73] The observation that CDW in ScV_6Sn_6 is suppressed in both cases suggests that a new model is needed to explain this behavior.

Let us begin by looking at how the rare earth atom size actually impacts the lattice. Figure 5 illustrates how the c and a lattice parameters of RV_6Sn_6 compounds depend on R at room temperature. First, observe that most of the lattice parameters of RV_6Sn_6 compounds (gray points) lie on a linear trend (dashed line) with the smaller, late rare earth atoms with smaller c and a. Sc is the smallest rare earth atom. If only the R size matters, we might expect the lattice parameters of ScV_6Sn_6 (dark green star) to lie on the lower left side of this trend. This is not the case. It has a smaller a but a comparable c to that of the Lu compound (purple star). Obviously, the lattice size is not simply controlled by the size of the rare earth atom. Our doping series emphasizes this anomalous lattice evolution in Figure 5 (small blue and purple symbols) as the lattice parameters interpolate between the end members.

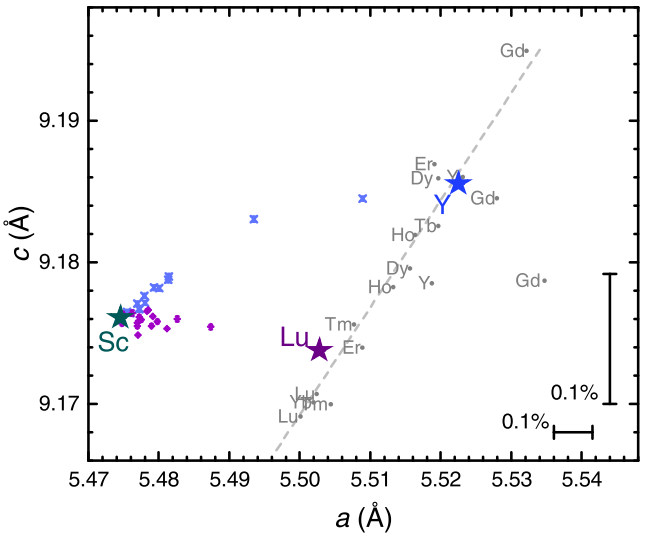

Figure 5. Comparison of room temperature c and a lattice parameters for doped ScV_6Sn_6 and other reported RV_6Sn_6. Gray dots label reported lattice parameters.[53,55,70,84] Stars represent the lattice parameters of ScV_6Sn_6, LuV_6Sn_6, and YV_6Sn_6 determined by powder XRD. The small purple and blue dots are the lattice parameters of the $(Sc,Lu)V_6Sn_6$ and $(Sc,Y)V_6Sn_6$ doping series, respectively.

Bonding Trends. We have established that the c lattice parameter has a nontrivial dependence on the rare earth ion. How are larger R atoms accommodated in the crystal structure if c is only weakly affected? Figure 6 presents the evolution of key bond distances with R ionic radius across the RV_6Sn_6 materials determined by single-crystal XRD. To begin, note that larger rare earth atoms produce a larger R−Sn1 bond distance (blue), but the c lattice parameter (black, plotted as $\left(\frac{c}{3}\right)$) increases far more slowly. This requires that the Sn1−Sn1 distance must decrease (red). In other words, larger rare earth atoms compress the Sn1−Sn1 bond with little impact on the unit cell height. Apparently, there is extra room in the R−Sn1−Sn1 chain to accommodate larger atoms.

Rattling Chain Model. What is setting the size of c if the R−Sn1−Sn1 chains do not? We propose that the stack of V-kagome and Sn2/Sn3-honeycomb sheets do. Start by considering the RV_6Sn_6 as two subsystems: R−Sn1−Sn1 chains filling tubes in a superstructure of stacked V-kagome and Sn-honeycomb sheets (illustrated in Figure 1b). Figure 7 depicts a cut along the (110) plane, presenting the sections of V and Sn sheets as colored rectangles.

ScV_6Sn_6 and LuV_6Sn_6 have nearly identical c values suggesting that the stacked Sn and V sheets are setting c and small Sc atoms leave the channels underfilled (Figure 7b). This facilitates low-energy rattling displacements of Sn1 and R atoms. This rattling is evident in the atomic displacement parameters (ADPs) from our single-crystal XRD refinements (Supporting Information). The c-axis displacement parameters, U_{33}, for the R and Sn1 atoms are twice as large in ScV_6Sn_6 than those in the Lu or Y compounds. We illustrate this difference in the inset of Figure 6 by depicting the 95% displacement ellipsoids for the R and Sn1 atoms. The Sc and Sn1 atoms in the first column show taller ellipsoids, representing larger position deviations in this direction. This reflects the strong CDW fluctuation observed in ScV_6Sn_6 by inelastic and diffuse X-ray scattering.[56,58,59]

https://doi.org/10.1021/jacs.3c06394
J. Am. Chem. Soc. 2023, 145, 20943−20950

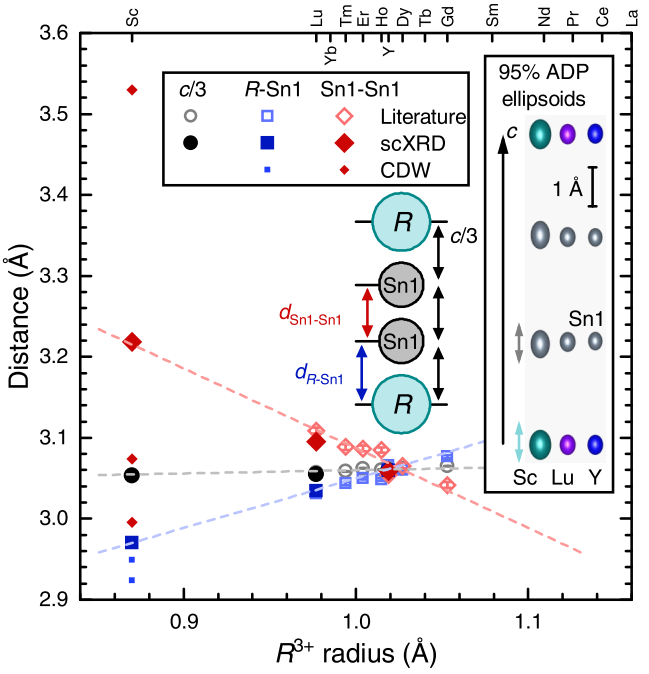

Figure 6. Evolution of bond distances with R^{3+} rare earth ionic radii (coordination number = 8 from Shannon et al.[80]). Large, pale-colored marks come from the literature.[53] Large solid symbols represent distances determined by single-crystal X-ray diffraction refinements in this study and Arachchige et al.[52] Tiny symbols present the Sn1−Sn1 (red) and R−Sn1 (blue) bond lengths in the CDW phase of ScV_6Sn_6.[52] The boxed inset depicts the 95% displacement ellipsoids of the R and Sn1 atoms in the refined structures of the Sc, Lu, and Y compounds. The atomic displacement parameters (ADPs) are plotted in the Supporting Information.

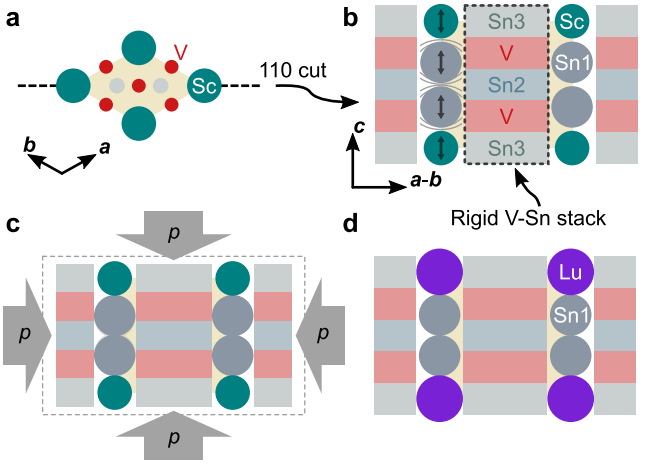

Figure 7. Cartoon of the R−Sn1−Sn1 stack. (a) View along [001] of the ScV_6Sn_6 structure. (b) (110) cut through the ScV_6Sn_6 structure depicting a rigid stack of V-kagome and Sn-honeycomb sheets (colored rectangles) and a loosely packed chain of Sc and Sn1 atoms, providing room for them to rattle along *c*. (c) Applying pressure compresses the lattice and removes the extra space in the Sc−Sn1−Sn1 chains. (d) Replacing Sc with larger Lu compresses the R−Sn1−Sn1 chain and removes the room for the atoms to rattle.

These are precisely the displacements that are most prominent in ScV_6Sn_6's CDW phase. The small symbols in Figure 6 are the bond lengths in the refined CDW structure of ScV_6Sn_6 from Arachchige et al.[52] The Sc−Sn1 bonds shrink a little (small blue dots) within the Sn1−Sc−Sn1 trimers highlighted by Pokharel et al.[56] The Sc−Sn bonding within these units appears unaltered by the CDW based on orbital contributions to bands at the Fermi surface.[66]

In contrast, the Sn1−Sn1 bonds are modified more dramatically (small red dots). Two Sn1−Sn1 distances shorten by 4.5 and 6.9%, while the final third of bonds grow by 9.7%. These Sn1−Sn1 bonds are key features of CDW and modify the Sn1 p_z orbital states.[56,59,65,66]

We propose that the CDW instability needs extra space in R−Sn1−Sn1 chains for the modulations of Sn1−Sn1 distances observed in the CDW. If the column is packed too tightly by larger R atoms or physical pressure, the displacements are penalized.

Next, we will examine how we might expect modifications of ScV_6Sn_6 to impact the loose chains of R−Sn1−Sn1 atoms and the CDW these facilitate. Applying pressure suppresses T_{CDW} to 0 K by 2.4 GPa.[73] Pressure compresses the stack of V and Sn sheets (Figure 7c). This constrains the chain of atoms, which shortens the Sn1−Sn1 bonds. The CDW is penalized as the extra room in the chain is removed.

Doping ScV_6Sn_6 with Lu and Y quickly kills the CDW. In this case, introducing larger atoms fills up the extra room in the R−Sn1−Sn1 chains (Figure 7d), compressing the Sn1−Sn1 bonds and suppressing the CDW instability. This explains not only why Lu and Y doping both suppresse the CDW but also why no CDW transition is observed in RV_6Sn_6 with R bigger than Sc.

This rattling chain mechanism is distinct from the familiar correspondence between chemical and physical pressure. The CDW in ScV_6Sn_6 is suppressed by both lattice compression (physical pressure) and expansion by Lu/Y doping. Our model predicts that pressure and doping by larger rare earth atoms should cooperate to reduce T_{CDW}.

Cooperative Effects of Pressure and Lu Doping. We test this prediction by monitoring the evolution of the transition temperature with pressure in a crystal where the CDW is already partly suppressed by Lu doping. Figure 8 presents the resistance versus temperature of $(Sc_{0.944}Lu_{0.056})V_6Sn_6$ at a series of pressures. Near atmospheric pressure (black), the CDW transition is observed as a hysteretic drop in resistance on cooling at roughly 64 K. This drop-like feature decreases in temperature as pressure is increased until it changes character to a jump up on cooling for the highest two pressures (observed in pure ScV_6Sn_6 under pressure too[73]). Applying pressure compresses the V−Sn stack around the already compacted R−Sn1−Sn1 chain in the Lu-doped sample, further penalizing the CDW displacements. This observation discredits the possibility that ScV_6Sn_6 has an optimal lattice volume for CDW formation. In that case, applying pressure to the Lu-doped sample should restabilize the CDW and increase T_{CDW}, but this is not what we observe (see the Supporting Information).

CONCLUSIONS

In conclusion, we explored how rare earth size impacts CDW formation in the RV_6Sn_6 family. Magnetization measurements on single crystals of $(Sc,Lu)V_6Sn_6$ and $(Sc,Y)V_6Sn_6$ revealed that the CDW transition temperature is reduced with increasing Lu and Y content. X-ray diffraction reveals enlightening lattice and bond-length trends. These observations and the evolution of the CDW under pressure motivate us to propose a rattling chain model for CDW formation in the

https://doi.org/10.1021/jacs.3c06394
J. Am. Chem. Soc. 2023, 145, 20943−20950

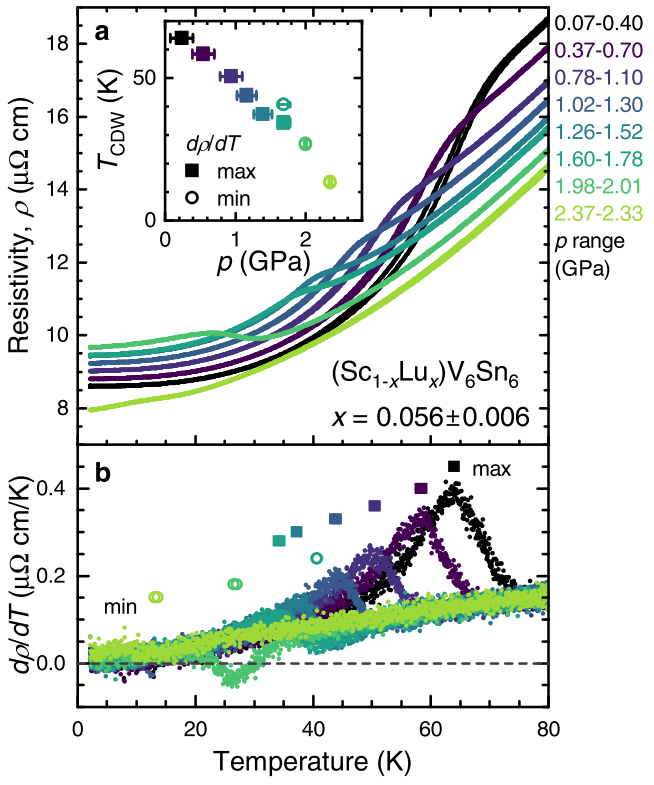

Figure 8. Pressure suppresses CDW in Lu-doped ScV_6Sn_6. (a) Resistivity vs temperature plots for $(Sc_{0.944}Lu_{0.056})V_6Sn_6$ at increasing pressures, p. Resistivity was measured with the current perpendicular to the c-axis. The pressures at low and high temperatures are listed on the right. The inset shows the pressure dependence of T_{CDW}. (b) Derivative of $\rho(T)$ highlighting maxima (squares) and minima (circles) used to define T_{CDW}.

RV_6Sn_6 compounds. We assert that a CDW is only observed in the Sc version of the RV_6Sn_6 compounds because the small Sc atom provides space for Sc and Sn1 atoms to rattle and permit the Sn1−Sn1 bond-length modulation observed in the low-temperature CDW phase. This model explains why both physical pressure and substitution of Sc by larger rare earth atoms suppress the CDW order. This is a curious variation to the common corresponding effects of chemical and physical pressure on phase stability. In addition to explaining why ScV_6Sn_6 is special, our observations and model provide an important leap forward in our understanding of CDWs in the intriguing kagome metals.

■ ASSOCIATED CONTENT

Supporting Information

The Supporting Information is available free of charge at https://pubs.acs.org/doi/10.1021/jacs.3c06394.

Refined structures of LuV_6Sn_6 and YV_6Sn_6 as well resistance under pressure measurements for LuV_6Sn_6 and $(Sc_{1-x}Lu_x)V_6Sn_6$ with $x = 0.180 \pm 0.019$; adiabatic demagnetization resistance measurements of doped ScV_6Sn_6 and LuV_6Sn_6 crystals are included as well; raw magnetization data behind the doping phase diagrams are presented along with an example how we estimated CDW transition temperature; LuV6Sn6_20230509.cif room-temperature single-crystal refinement of LuV_6Sn_6; YV6Sn6_20230519.cif room-temperature single crystal refinement of YV_6Sn_6 (PDF)

Accession Codes

CCDC 2270479−2270480 contain the supplementary crystallographic data for this paper. These data can be obtained free of charge via www.ccdc.cam.ac.uk/data_request/cif, or by emailing data_request@ccdc.cam.ac.uk, or by contacting The Cambridge Crystallographic Data Centre, 12 Union Road, Cambridge CB2 1EZ, UK; fax: +44 1223 336033.

■ AUTHOR INFORMATION

Corresponding Authors

William R. Meier − *Materials Science & Engineering Department, University of Tennessee Knoxville, Knoxville, Tennessee 37996, United States;* orcid.org/0000-0002-4060-5093; Email: javamocham@gmail.com

David Mandrus − *Department of Physics & Astronomy, University of Tennessee Knoxville, Knoxville, Tennessee 37996, United States;* orcid.org/0000-0003-3616-7104; Email: dmandrus@utk.edu

Authors

Richa Pokharel Madhogaria − *Materials Science & Engineering Department, University of Tennessee Knoxville, Knoxville, Tennessee 37996, United States*

Shirin Mozaffari − *Materials Science & Engineering Department, University of Tennessee Knoxville, Knoxville, Tennessee 37996, United States*

Madalynn Marshall − *Neutron Scattering Division, Oak Ridge National Laboratory, Oak Ridge, Tennessee 37831, United States*

David E. Graf − *National High Magnetic Field Laboratory, Tallahassee, Florida 32310, United States*

Michael A. McGuire − *Material Science & Technology Division, Oak Ridge National Laboratory, Oak Ridge, Tennessee 37831, United States;* orcid.org/0000-0003-1762-9406

Hasitha W. Suriya Arachchige − *Department of Physics & Astronomy, University of Tennessee Knoxville, Knoxville, Tennessee 37996, United States*

Caleb L. Allen − *Department of Physics & Astronomy, University of Tennessee Knoxville, Knoxville, Tennessee 37996, United States*

Jeremy Driver − *Department of Physics & Astronomy, University of Tennessee Knoxville, Knoxville, Tennessee 37996, United States*

Huibo Cao − *Neutron Scattering Division, Oak Ridge National Laboratory, Oak Ridge, Tennessee 37831, United States*

Complete contact information is available at: https://pubs.acs.org/10.1021/jacs.3c06394

Notes

The authors declare no competing financial interest.

■ ACKNOWLEDGMENTS

We thank Bryan C. Chakoumakos of the Oak Ridge National Laboratory for his helpful discussions with the single-crystal X-ray refinements and Adam Malin for creating cover art for this paper. M.A.M. and D.M. acknowledge support from the US Department of Energy, Office of Science, Basic Energy Sciences, Materials Sciences, and Engineering Division. W.R.M., H.W.S.A., C.L.A., and J.D. acknowledge support from the Gordon and Betty Moore Foundation's EPiQS Initiative, Grant GBMF9069 to D.M. S.M. and R.P.M.

acknowledge the support from AFOSR MURI (Novel Light−Matter Interactions in Topologically Non-Trivial Weyl Semimetal Structures and Systems) grant# FA9550-20-1-0322. M.M. and H.B.C. were supported by the U.S. Department of Energy (DOE), Office of Science, Office of Basic Energy Sciences, Early Career Research Program Award KC0402020, under Contract DE-AC05-00OR22725. A portion of this research used resources at the Spallation Neutron Source, a DOE Office of Science User Facility operated by the Oak Ridge National Laboratory. A portion of this work was performed at the National High Magnetic Field Laboratory, which is supported by National Science Foundation Cooperative Agreement No. DMR-2128556 and the State of Florida.

REFERENCES

(1) Zhu, X.; Guo, J.; Zhang, J.; Plummer, E. W. *Adv. Phys.: X* **2017**, *2*, 622−640, DOI: 10.1080/23746149.2017.1343098.
(2) Grüner, G. *Density Waves in Solids*; Perseus Publishing: Cambridge, Mass., 1994.
(3) Morosan, E.; Zandbergen, H. W.; Dennis, B. S.; Bos, J. W. G.; Onose, Y.; Klimczuk, T.; Ramirez, A. P.; Ong, N. P.; Cava, R. J. *Nat. Phys.* **2006**, *2*, 544−550, DOI: 10.1038/nphys360.
(4) Joe, Y. I.; Chen, X. M.; Ghaemi, P.; Finkelstein, K. D.; de la Peña, G. A.; Gan, Y.; Lee, J. C. T.; Yuan, S.; Geck, J.; MacDougall, G. J.; Chiang, T. C.; Cooper, S. L.; Fradkin, E.; Abbamonte, P. *Nat. Phys.* **2014**, *10*, 421−425, DOI: 10.1038/nphys2935.
(5) Boubeche, M.; Yu, J.; Chushan, L.; Huichao, W.; Zeng, L.; He, Y.; Wang, X.; Su, W.; Wang, M.; Yao, D.-X.; Wang, Z.; Luo, H. *Chin. Phys. Lett.* **2021**, *38*, No. 037401, DOI: 10.1088/0256-307X/38/3/037401.
(6) Kazama, T.; Maeda, M.; Takase, K.; Takano, Y.; Watanabe, T. *Solid State Phenom.* **2016**, *257*, 34−37, DOI: 10.4028/www.scientific.net/ssp.257.34.
(7) Sangeetha, N. S.; Thamizhavel, A.; Tomy, C. V.; Basu, S.; Awasthi, A. M.; Ramakrishnan, S.; Pal, D. *Phys. Rev. B* **2012**, *86*, No. 024524, DOI: 10.1103/PhysRevB.86.024524.
(8) Li, Z.; Chen, X.; Liu, X.; et al. *J. Alloys Compd.* **2023**, *937*, No. 168337, DOI: 10.1016/j.jallcom.2022.168337.
(9) Veiga, L. S. I.; Mardegan, J. R. L.; v Zimmermann, M.; Maimone, D. T.; Carneiro, F. B.; Fontes, M. B.; Strempfer, J.; Granado, E.; Pagliuso, P. G.; Bittar, E. M. *Phys. Rev. B* **2020**, *101*, No. 104511, DOI: 10.1103/physrevb.101.104511.
(10) Goh, S. K.; Tompsett, D. A.; Saines, P. J.; Chang, H. C.; Matsumoto, T.; Imai, M.; Yoshimura, K.; Grosche, F. M. *Phys. Rev. Lett.* **2015**, *114*, No. 097002, DOI: 10.1103/PhysRevLett.114.097002.
(11) Klintberg, L. E.; Goh, S. K.; Alireza, P. L.; Saines, P. J.; Tompsett, D. A.; Logg, P. W.; Yang, J.; Chen, B.; Yoshimura, K.; Grosche, F. M. *Phys. Rev. Lett.* **2012**, *109*, No. 237008, DOI: 10.1103/PhysRevLett.109.237008.
(12) Sipos, B.; Kusmartseva, A. F.; Akrap, A.; Berger, H.; Forró, L.; Tutiš, E. *Nat. Mater.* **2008**, *7*, 960−965, DOI: 10.1038/nmat2318.
(13) Briggs, A.; Monceau, P.; Nunez-Regueiro, M.; Peyrard, J.; Ribault, M.; Richard, J. *J. Phys. C: Solid State Phys.* **1980**, *13*, 2117−2130, DOI: 10.1088/0022-3719/13/11/011.
(14) Zocco, D. A.; Hamlin, J. J.; Grube, K.; Chu, J.-H.; Kuo, H.-H.; Fisher, I. R.; Maple, M. B. *Phys. Rev. B* **2015**, *91*, No. 205114, DOI: 10.1103/PhysRevB.91.205114.
(15) Zeng, L.; Yan, D.; He, Y.; Boubeche, M.; Huang, Y.; Wang, X.; Luo, H. *J. Alloys Compd.* **2021**, *885*, No. 160981, DOI: 10.1016/j.jallcom.2021.160981.
(16) Aulestia, E. I. P.; Liu, X.; Pang, Y. Y.; So, C. W.; Yu, W. C.; Goh, S. K.; Lai, K. T. *J. Phys.: Condens.Matter* **2021**, *34*, No. 06LT01, DOI: 10.1088/1361-648x/ac34af.
(17) Eckberg, C.; Campbell, D. J.; Metz, T.; Collini, J.; Hodovanets, H.; Drye, T.; Zavalij, P.; Christensen, M. H.; Fernandes, R. M.; Lee, S.; Abbamonte, P.; Lynn, J. W.; Paglione, J. *Nat. Phys.* **2020**, *16*, 346−350, DOI: 10.1038/s41567-019-0736-9.
(18) Lee, S.; de la Peña, G.; Sun, S. X.-L.; Mitrano, M.; Fang, Y.; Jang, H.; Lee, J.-S.; Eckberg, C.; Campbell, D.; Collini, J.; Paglione, J.; de Groot, F. M. F.; Abbamonte, P. *Phys. Rev. Lett.* **2019**, *122*, No. 147601, DOI: 10.1103/PhysRevLett.122.147601.
(19) Kudo, K.; Takasuga, M.; Okamoto, Y.; Hiroi, Z.; Nohara, M. *Phys. Rev. Lett.* **2012**, *109*, No. 097002, DOI: 10.1103/PhysRevLett.109.097002.
(20) Momma, K.; Izumi, F. *J. Appl. Crystallogr.* **2011**, *44*, 1272−1276, DOI: 10.1107/S0021889811038970.
(21) Teng, X.; Oh, J. S.; Tan, H.; et al. *Nat. Phys.* **2023**, *19*, 814−822, DOI: 10.1038/s41567-023-01985-w.
(22) Meier, W. R.; Du, M.-H.; Okamoto, S.; Mohanta, N.; May, A. F.; McGuire, M. A.; Bridges, C. A.; Samolyuk, G. D.; Sales, B. C. *Phys. Rev. B* **2020**, *102*, No. 075148, DOI: 10.1103/PhysRevB.102.075148.
(23) Liang, Z.; Hou, X.; Zhang, F.; Ma, W.; Wu, P.; Zhang, Z.; Yu, F.; Ying, J.-J.; Jiang, K.; Shan, L.; Wang, Z.; Chen, X.-H. *Phys. Rev. X* **2021**, *11*, No. 031026, DOI: 10.1103/PhysRevX.11.031026.
(24) Kang, M.; Fang, S.; Kim, J.-K.; et al. *Nat. Phys.* **2022**, *18*, 301−308, DOI: 10.1038/s41567-021-01451-5.
(25) Ortiz, B. R.; Teicher, S. M. L.; Kautzsch, L.; Sarte, P. M.; Ratcliff, N.; Harter, J.; Ruff, J. P. C.; Seshadri, R.; Wilson, S. D. *Phys. Rev. X* **2021**, *11*, No. 041030, DOI: 10.1103/PhysRevX.11.041030.
(26) Hu, Y.; Wu, X.; Ortiz, B. R.; Ju, S.; Han, X.; Ma, J.; Plumb, N. C.; Radovic, M.; Thomale, R.; Wilson, S. D.; Schnyder, A. P.; Shi, M. *Nat. Commun.* **2022**, *13*, No. 2220, DOI: 10.1038/s41467-022-29828-x.
(27) Mozaffari, S.; Meier, W. R.; Madhogaria, R. P.et al. Universal sublinear resistivity in vanadium kagome materials hosting charge density waves. 2023, arXiv:2305.02393. arXiv.org e-Printarchive. https://arxiv.org/abs/2305.02393. (Accessed August 1, 2023).
(28) Colman, R. H.; Sinclair, A.; Wills, A. S. *Chem. Mater.* **2011**, *23*, 1811−1817, DOI: 10.1021/cm103160q.
(29) Wang, Y.; McCandless, G. T.; Wang, X.; Thanabalasingam, K.; Wu, H.; Bouwmeester, D.; van der Zant, H. S. J.; Ali, M. N.; Chan, J. Y. *Chem. Mater.* **2022**, *34*, 7337−7343, DOI: 10.1021/acs.chemmater.2c01309.
(30) Miiller, W.; Christensen, M.; Khan, A.; Sharma, N.; Macquart, R. B.; Avdeev, M.; McIntyre, G. J.; Piltz, R. O.; Ling, C. D. *Chem. Mater.* **2011**, *23*, 1315−1322, DOI: 10.1021/cm1034003.
(31) Gui, X.; Cava, R. J. *Chem. Mater.* **2022**, *34*, 2824−2832, DOI: 10.1021/acs.chemmater.2c00280.
(32) Allison, M. C.; Wurmehl, S.; Büchner, B.; Vella, J. L.; Söhnel, T.; Bräuninger, S. A.; Klauss, H.-H.; Avdeev, M.; Marlton, F. P.; Schmid, S.; Ling, C. D. *Chem. Mater.* **2022**, *34*, 1369−1375, DOI: 10.1021/acs.chemmater.1c04060.
(33) Sales, B. C.; Meier, W. R.; Parker, D. S.; et al. *Chem. Mater.* **2022**, *34*, 7069−7077, DOI: 10.1021/acs.chemmater.2c01634.
(34) Thakur, G. S.; Vir, P.; Guin, S. N.; Shekhar, C.; Weihrich, R.; Sun, Y.; Kumar, N.; Felser, C. *Chem. Mater.* **2020**, *32*, 1612−1617, DOI: 10.1021/acs.chemmater.9b05009.
(35) McGuire, M. A.; Zhang, Q.; Miao, H.; Luo, W.; Yoon, M.; Liu, Y.; Yilmaz, T.; Vescovo, E. *Chem. Mater.* **2021**, *33*, 9741−9749, DOI: 10.1021/acs.chemmater.1c03596.
(36) Meschke, V.; Gorai, P.; Stevanović, V.; Toberer, E. S. *Chem. Mater.* **2021**, *33*, 4373−4381, DOI: 10.1021/acs.chemmater.1c00071.
(37) Jovanovic, M.; Schoop, L. M. *J. Am. Chem. Soc.* **2022**, *144*, 10978−10991.
(38) Ortiz, B. R.; Gomes, L. C.; Morey, J. R.; Winiarski, M.; Bordelon, M.; Mangum, J. S.; Oswald, I. W. H.; Rodriguez-Rivera, J. A.; Neilson, J. R.; Wilson, S. D.; Ertekin, E.; McQueen, T. M.; Toberer, E. S. *Phys. Rev. Mater.* **2019**, *3*, No. 094407.
(39) Ortiz, B. R.; Sarte, P. M.; Kenney, E. M.; Graf, M. J.; Teicher, S. M. L.; Seshadri, R.; Wilson, S. D. *Phys. Rev. Mater.* **2021**, *5*, No. 034801.
(40) Ortiz, B. R.; Teicher, S. M. L.; Hu, Y.; Zuo, J. L.; Sarte, P. M.; Schueller, E. C.; Abeykoon, A. M. M.; Krogstad, M. J.; Rosenkranz, S.; Osborn, R.; Seshadri, R.; Balents, L.; He, J.; Wilson, S. D. *Phys. Rev. Lett.* **2020**, *125*, No. 247002.
(41) Nie, L.; Sun, K.; Ma, W.; et al. *Nature* **2022**, *604*, 59−64.

(42) Wang, Z.; Jiang, Y.-X.; Yin, J.-X.; et al. *Phys. Rev. B* **2021**, *104*, No. 075148.
(43) Li, H.; Zhang, T. T.; Yilmaz, T.; et al. *Phy. Rev. X* **2021**, *11*, No. 031050.
(44) Yu, F. H.; Wu, T.; Wang, Z. Y.; Lei, B.; Zhuo, W. Z.; Ying, J. J.; Chen, X. H. *Phys. Rev. B* **2021**, *104*, No. l041103.
(45) Jiang, Y.-X.; Yin, J.-X.; Denner, M. M.; et al. *Nat. Mater.* **2021**, *20*, 1353−1357.
(46) Yang, S.-Y.; Wang, Y.; Ortiz, B. R.; Liu, D.; Gayles, J.; Derunova, E.; Gonzalez-Hernandez, R.; Šmejkal, L.; Chen, Y.; Parkin, S. S. P.; Wilson, S. D.; Toberer, E. S.; McQueen, T.; Ali, M. N. *Sci. Adv.* **2020**, *6*, No. eabb6003, DOI: 10.1126/sciadv.abb6003.
(47) Yu, F. H.; Ma, D. H.; Zhuo, W. Z.; Liu, S. Q.; Wen, X. K.; Lei, B.; Ying, J. J.; Chen, X. H. *Nat. Commun.* **2021**, *12*, No. 3645, DOI: 10.1038/s41467-021-23928-w.
(48) Du, F.; Luo, S.; Ortiz, B. R.; Chen, Y.; Duan, W.; Zhang, D.; Lu, X.; Wilson, S. D.; Song, Y.; Yuan, H. *Phys. Rev. B* **2021**, *103*, No. l220504.
(49) Oey, Y. M.; Ortiz, B. R.; Kaboudvand, F.; Frassineti, J.; Garcia, E.; Cong, R.; Sanna, S.; Mitrović, V. F.; Seshadri, R.; Wilson, S. D. *Phys. Rev. Mater.* **2022**, *6*, No. l041801.
(50) Yin, Q.; Tu, Z.; Gong, C.; Fu, Y.; Yan, S.; Lei, H. *Chin. Phys. Lett.* **2021**, *38*, No. 037403.
(51) Wang, N.; Gu, Y.; McGuire, M. A.; et al. *Chin. Phys. B* **2022**, *31*, No. 017106.
(52) Arachchige, H. W. S.; Meier, W. R.; Marshall, M.; Matsuoka, T.; Xue, R.; McGuire, M. A.; Hermann, R. P.; Cao, H.; Mandrus, D. *Phys. Rev. Lett.* **2022**, *129*, No. 216402.
(53) Romaka, L.; Stadnyk, Y.; Romaka, V.; Demchenko, P.; Stadnyshyn, M.; Konyk, M. *J. Alloys Compd.* **2011**, *509*, 8862−8869.
(54) Zhang, X. X.; Liu, Z. Y.; Cui, Q.; Wang, N. N.; Shi, L. F.; Zhang, H.; Dong, X. L.; Sun, J. P.; Dun, Z. L.; Cheng, J. G. Electronic and magnetic properties of intermetallic kagome magnets RV_6Sn_6 (*R* = Tb - Tm). 2022, arXiv:2206.05653. arXiv.org e-Printarchive https://arxiv.org/abs/2206.05653. (Accessed August 2, 2023).
(55) Lee, J.; Mun, E. *Phys. Rev. Materials* **2022**, *6*, No. 083401.
(56) Pokharel, G.; Ortiz, B. R.; Kautzsch, L.; Alvarado, S. J. G.; Mallayya, K.; Wu, G.; Kim, E.-A.; Ruff, J. P. C.; Sarker, S.; Wilson, S. D. Frustrated charge order and cooperative distortions in ScV_6Sn_6. 2023, arXiv:2307.11843. arXiv.org e-Printarchive. https://arxiv.org/abs/2307.11843. (Accessed August 2, 2023).
(57) Tan, H.; Yan, B. *Phys. Rev. Lett.* **2023**, *130*, No. 266402.
(58) Cao, S.; Xu, C.; Fukui, H.; Manjo, T.; Shi, M.; Liu, Y.; Cao, C.; Song, Y. Competing charge-density wave instabilities in the kagome metal ScV_6Sn_6. 2023, arXiv:2304.08197. arXiv.org e-Printarchive. https://arxiv.org/abs/2304.08197. (Accessed August 2, 2023).
(59) Korshunov, A.; Hu, H.; Subires, D.et al. Softening of a flat phonon mode in the kagome ScV_6Sn_6. 2023, arXiv:2304.09173. arXiv.org e-Printarchive. https://arxiv.org/abs/2304.09173. (Accessed August 2, 2023).
(60) Neupert, T.; Denner, M. M.; Yin, J.-X.; Thomale, R.; Hasan, M. Z. *Nat. Phys.* **2022**, *18*, 137−143.
(61) Mu, C.; Yin, Q.; Tu, Z.; Gong, C.; Lei, H.; Li, Z.; Luo, J. *Chin. Phys. Lett.* **2021**, *38*, No. 077402.
(62) Cheng, S.; Ren, Z.; Li, H.et al. Nanoscale visualization and spectral fingerprints of the charge order in ScV_6Sn_6 distinct from other kagome metals. 2023, arXiv:2302.12227. arXiv.org e-Printarchive. https://arxiv.org/abs/2302.12227.(Accessed August 2, 2023).
(63) Kang, S.-H.; Li, H.; Meier, W. R.; Villanova, J. W.; Hus, S.; Jeon, H.; Arachchige, H. W. S.; Lu, Q.; Gai, Z.; Denlinger, J.; Moore, R.; Yoon, M.; Mandrus, D. Emergence of a new band and the Lifshitz transition in kagome metal ScV_6Sn_6 with charge density wave. 2023, arXiv:2302.14041. arXiv.org e-Printarchive. https://arxiv.org/abs/2302.14041. (Accessed August 2, 2023).
(64) Hu, Y.et al. Phonon promoted charge density wave in topological kagome metal ScV_6Sn_6. 2023, arXiv:2304.06431. arXiv.org e-Printarchive. https://arxiv.org/abs/2304.06431. (Accessed August 2, 2023).
(65) Lee, S.; Won, C.; Kim, J.; Yoo, J.; Park, S.; Denlinger, J.; Jozwiak, C.; Bostwick, A.; Rotenberg, E.; Comin, R.; Kang, M.; Park, J.-H. Nature of charge density wave in kagome metal ScV_6Sn_6. 2023, arXiv:2304.11820. arXiv.org e-Printarchive. https://arxiv.org/abs/2304.11820. (Accessed August 2, 2023).
(66) Hu, H.; Jiang, Y.; Călugăru, D.; Feng, X.; Subires, D.; Vergniory, M. G.; Felser, C.; Blanco-Canosa, S.; Bernevig, B. A. Kagome materials I: SG 191, ScV_6Sn_6. Flat phonon soft modes and unconventional CDW formation: Microscopic and effective theory. 2023, arXiv:2305.15469. arXiv.org e-Printarchive https://arxiv.org/abs/2305.15469. (Accessed August 2, 2023).
(67) Yi, C.; Feng, X.; Yanda, P.; Roychowdhury, S.; Felser, C.; Shekhar, C. Charge density wave induced anomalous Hall effect in kagome ScV_6Sn_6. 2023, arXiv:2305.04683. arXiv.org e-Printarchive. https://arxiv.org/abs/2305.04683. (Accessed August 2, 2023).
(68) Guguchia, Z.; Gawryluk, D. J.; Shin, S.et al. Hidden magnetism uncovered in charge ordered bilayer kagome material ScV_6Sn_6. 2023, arXiv:2304.06436.arXiv.org e-Printarchive. https://arxiv.org/abs/2304.06436. (Accessed August 2, 2023).
(69) Pokharel, G.; Ortiz, B.; Chamorro, J.; Sarte, P.; Kautzsch, L.; Wu, G.; Ruff, J.; Wilson, S. D. *Phys. Rev. Mater.* **2022**, *6*, No. 104202.
(70) Pokharel, G.; Teicher, S. M. L.; Ortiz, B. R.; Sarte, P. M.; Wu, G.; Peng, S.; He, J.; Seshadri, R.; Wilson, S. D. *Phys. Rev. B* **2021**, *104*, No. 235139.
(71) Ishikawa, H.; Yajima, T.; Kawamura, M.; Mitamura, H.; Kindo, K. *J. Phys. Soc. Jpn.* **2021**, *90*, No. 124704.
(72) Rosenberg, E.; DeStefano, J. M.; Guo, Y.; Oh, J. S.; Hashimoto, M.; Lu, D.; Birgeneau, R. J.; Lee, Y.; Ke, L.; Yi, M.; Chu, J.-H. *Phys. Rev. B* **2022**, *106*, No. 115139.
(73) Zhang, X.; Hou, J.; Xia, W.; Xu, Z.; Yang, P.; Wang, A.; Liu, Z.; Shen, J.; Zhang, H.; Dong, X.; Uwatoko, Y.; Sun, J.; Wang, B.; Guo, Y.; Cheng, J. *Materials* **2022**, *15*, No. 7372.
(74) Canfield, P. C.; Kong, T.; Kaluarachchi, U. S.; Jo, N. H. *Philos. Mag.* **2016**, *96*, 84−92.
(75) CrysAlisPRO. Oxford Diffraction/Agilent Technologies UK Ltd., Yarnton, England
(76) Sheldrick, G. M. *Acta Crystallogr., Sect. C: Struct. Chem.* **2015**, *71*, 3−8.
(77) Sheldrick, G. M. *Acta Crystallogr., Sect. A: Found. Adv.* **2015**, *71*, 3−8.
(78) Staško, D.; Prchal, J.; Klicpera, M.; Aoki, S.; Murata, K. *High Pressure Res.* **2020**, *40*, 525−536.
(79) Piermarini, G. J.; Block, S.; Barnett, J. D.; Forman, R. A. *J. Appl. Phys.* **1975**, *46*, 2774−2780.
(80) Shannon, R. D. *Acta Crystallogr., Sect. A* **1976**, *A32*, 751−767.
(81) Kittel, C. *Introduction to Solid State Physics*, 8th ed.; John Wiley & Sons Inc: Hoboken, NJ, 2004.
(82) Coleman, P.; Schofield, A. J. *Nature* **2005**, *433*, 226−229.
(83) Sinha, M.; Vivanco, H. K.; Wan, C.; Siegler, M. A.; Stewart, V. J.; Pogue, E. A.; Pressley, L. A.; Berry, T.; Wang, Z.; Johnson, I.; Chen, M.; Tran, T. T.; Phelan, W. A.; McQueen, T. M. *ACS Cent. Sci.* **2021**, *7*, 1381−1390.
(84) Guo, K.; Ye, J.; Guan, S.; Jia, S. *Phys. Rev. B* **2023**, *107*, No. 205151.

https://doi.org/10.1021/jacs.3c06394
J. Am. Chem. Soc. 2023, 145, 20943−20950